Int J Adv Manuf Technol (2017) 92:1923–1931
DOI 10.1007/s00170-017-0310-5

ORIGINAL ARTICLE

Microstructure and fatigue behavior of resistance element welded dissimilar joints of DP780 dual-phase steel to 6061-T6 aluminum alloy

Zhanxiang Ling[1] · Yang Li[1] · Zhen Luo[1,2] · Sansan Ao[1] · Zhanghua Yin[3] · Yunlong Gu[4] · Qiang Chen[5]

Received: 13 October 2016 / Accepted: 14 March 2017 / Published online: 23 March 2017

Abstract A novel resistance element welding was employed for dissimilar joining of electro-galvanized DP780 steel to 6061-T6 aluminum alloy. Compared with traditional resistance spot welding, the change of load bearing part resulted in higher joint strength and energy absorption capacity. Microstructures of dissimilar joints vary according to the distance from the weld center. Intermetallic compound layers were formed at the Al/rivet interface and Al/steel interface in the resistance element welding joints and resistance spot welding joints, respectively. The fatigue strength, and fatigue fractographs of the dissimilar joints were obtained and discussed. Resistance element welding joints showed higher fatigue strength than resistance spot welding joints, with the fatigue limit of 1800 and 900 N, respectively. The fatigue fracture modes of both types of joints were dependent on the load levels. At high load levels, the REW joints and RSW joints underwent pull-out and interfacial fracture, respectively. At low load levels, both joints underwent through-thickness fracture.

✉ Zhen Luo
lz_tju@163.com

✉ Sansan Ao
ao33@tju.edu.cn

[1] School of Materials Science and Engineering, Tianjin University, 31-291, No.135 Yaguan Road, Tianjin 300350, China

[2] Collaborative Innovation Center of Advanced Ship and Deep-Sea Exploration, Shanghai 200240, China

[3] National Engineering Laboratory for Pineline Safety, Langfang 065001, China

[4] Pipeline Research Institute of CNPC, Langfang 065001, China

[5] Ansteel Mining Engineering Corporation, Anshan 114004, China

Keywords Resistance element welding · Aluminum alloy · Dual-phase steel · Microstructure · Microhardness · Fatigue strength

1 Introduction

Rapid economic development has been accompanied by environmental concerns. Industries have attempted to save energy and reduce greenhouse gas emissions, especially in the automobile industry, because rigorous laws restricting automobile emissions have been instituted [1]. In addition to changes in the car shape and improving the powertrain, weight reduction may be used to meet the requirements, as the petrol consumption and, in turn, emissions will decrease with decreasing weight of the car [2]. The need for reduced emissions has resulted in the gradual use of light-weight materials such as aluminum (Al) and magnesium (Mg) in the automotive industry. Companies such as Audi have successfully developed an aluminum space frame (ASF). However, steels are still the dominant materials used in automobiles owing to their low price, high strength and hardness, excellent dimensional accuracy, and formability. In this case, a multi-material-designed car body should provide a balanced solution and therefore, joining dissimilar materials (especially aluminum to steel) constitutes a reliable method for realizing this solution.

Resistance spot welding (RSW) is a critical and widely used joining technique in the automotive industry, which attributed to its low cost, efficiency, and mature technology [3]. An automobile contains approximately 3000–7000 spot welds [4] and, hence, researchers initially introduced the RSW method for joining Al to steel. However, unlike similar materials, Al and steel have significantly differing properties; for example, the melting point of steel is ~2.5 times that of Al. In

Table 1 Chemical composition of materials/wt-%

Materials	Cu	Mg	Zn	Ti	Cr	C	P	S	Si	Mn	Fe	Al
Al 6061	0.18	0.86	0.25	0.10	0.05	–	–	–	0.48	0.15	0.7	Bal.
DP780	0.001	–	–	0.024	0.326	0.08	0.007	0.002	0.18	2.08	Bal.	0.03
Q235	–	–	–	–	–	0.14	0.04	0.02	0.4	1.0	Bal.	–

addition, the thermal expansion, thermal conductivity, and modulus of elasticity of Al are approximately two, six, and three times, respectively, those of steel. The solubility between Al and steel is nearly zero [5]. Consequently, an Al-Fe intermetallic compound (IMC) is formed when Al is welded to steel. The IMC layer at the Al/Fe interface is rather brittle. The thickness of this layer has a significant effect on the joint quality, and excellent mechanical strength can be achieved for thicknesses ranging from 5 to 10 μm [6]. Several attempts have been made to control the IMC layer thickness during RSW [7–11]. In addition, owing to its excellent metallurgical compatibility with both materials, researchers has found that the hot-dipped zinc coating on steel plays an important role in improving the Al/steel dissimilar joint strength; melting and evaporation of the coating leads to a decrease in the Al-Fe IMC layer thickness [5, 12]. Thus, the joining of Al to hot-dipped-zinc-coated steel has therefore been extensively investigated [9, 10, 13]. Uncoated steel and electro-galvanized steel (its Zn coating is rather thin so the effect is limited) are also widely used in industry. However, the joining of these materials to Al remains challenging.

To effectively control the IMC layer thickness or avoid the formation of this layer altogether, other spot joining methods for joining Al to steel have been proposed. These methods include cold metal transfer spot plug welding [14], friction stir spot welding (FSSW) [15], ultrasonic spot welding [16], self-piercing riveting (SPR) [17], clinching [18], and friction bit joining [19]. Although acceptable Al/steel dissimilar joints can be obtained by using these methods, drawbacks still persist. For example, the relatively low efficiency of cold metal transfer spot plug welding prevents its use in mass production; the low power of the ultrasonic spot welding machine renders it suitable mainly for welding thin or soft sheets; the equipment used for FSSW is quite complex; SPR is just as productive as RSW, but large deformation and insufficient penetration occur during the joining of low-formability advanced high-strength steel [20].

The authors recently realized excellent dissimilar welding by using a novel method, i.e., resistance element welding (REW), to weld uncoated 22MnMoB boron steel to 6061-T6 aluminum alloy [21]. Using this method, a traditional RSW machine can be used to join non-ferrous material to ferrous material. In dissimilar Al/steel REW joint, the IMC layer was replaced by steel nugget to bear the load, thereby fundamentally preventing the harmful effect of the IMC layer. In the current work, the authors developed an electro-galvanized DP780 dual-phase steel/6061-T6 aluminum alloy dissimilar joints using the REW method and researched its microstructure, microhardness, and fatigue behavior. As far as the authors know, the fatigue behavior of REW dissimilar joints has never been studied before. RSW dissimilar joints were also studied with the purpose of comparison.

2 Materials and method

A 2-mm-thick 6061-T6 Al alloy and a 1.4-mm-thick electro-galvanized DP780 dual-phase steel were used as the base metals, and the Q235 steel rivets with the diameter of 5 mm were used as the auxiliary elements. The chemical compositions of used materials are listed in Table 1.

The REW process is shown in Fig. 1. A hole located at the welding site was previously drilled in the Al sheet and a rivet was subsequently inserted into the hole; the bottom of the rivet and the bottom of the Al sheet were kept in the identical plane. The welding procedure was then performed at the location of the rivet, using a 220-kW medium frequency direct current resistance spot welding machine, capable of generating a welding current of 2–22 kA. A copper–chromium conical electrode and a domed electrode were used for the top and bottom sides, respectively.

Figure 2 shows the configuration of the REW joints subjected to tensile shear tests. The Al and steel sheets were cut to a size of 100 × 25 mm, in accordance with the AWS-D17.2 standard [22], and the rivet was placed in the center of a 25-mm overlap region. For comparison, the same configuration

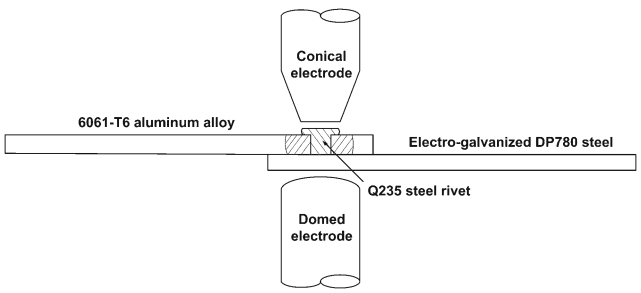

Fig. 1 Schematic of the resistance element welding process

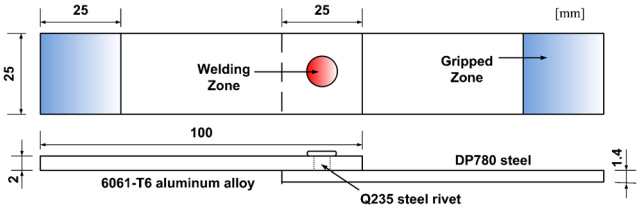

Fig. 2 Tensile shear specimen of the REW joint

was used for both the REW and RSW joints (in both cases, the welding procedure was performed at the center of the 25-mm overlap region).

After welding, the peak load of the joints was obtained via tensile shear tests performed on a CSS-44100 material test system operated at a constant crosshead velocity of 1 mm/min. The area under the load-displacement diagram was measured to determine the energy absorption of the joints prior to failure [23]. The cross-section of the joints was determined from specimens cut by a wire cutting machine. These specimens were then prepared via standard metallographic procedures: the steel was etched for 2 s in a 4% nital solution, whereas the Al was etched for 15 s in Keller's reagent. The profile and microstructure of the joints were examined by using an Olympus SZX12 stereomicroscope and an Olympus GX51 metallographic microscope, respectively. Fractography (Hitachi S-1510 scanning electron microscope (SEM)) and elemental composition analysis (Hitachi S-4800 SEM equipped with a Genesis XM2 energy dispersive spectrometer (EDS)) were also conducted. Similarly, 10-s microhardness measurements (HUAYIN HV-1000A micro Vickers hardness tester) were performed at loads of 200 and 50 g for steel and Al, respectively. The tension-tension fatigue test of the optimized joints was conducted on an MTS 810 Material Test System, with the sinusoidal waveform in load-control mode at a stress ratio of $R = 0.1$. The frequency ranged from 10 to 30 Hz, depending on the load level. To compensate for the thickness offset, a steel shim and an Al shim were used at the grip zone of the Al sheet and steel sheet, respectively.

3 Results and discussion

3.1 Pretensile shear test under quasi-static loading

To determine the load levels during fatigue test, tensile shear test was carried out firstly on REW and RSW dissimilar joints. Based on preliminary test, 300 ms and 6–10 kA (with an interval of 1 kA) were used as the welding time and welding current, respectively, during the REW process, and a welding time of 200 ms and a welding current of 12–16 kA (with an interval of 1 kA) were used during the RSW process. The upper electrode tip diameters were 10 and 6 mm for the REW and RSW processes, respectively, and the electrode force was set to 3.6 kN for both joints. The results are shown in Fig. 3. Overall, both tensile strength and energy absorption of REW joints (with a maximum value of 7368 N and 18.9 J respectively) were much higher than RSW joints (with a maximum value of 4332 N and 2.9 J respectively). And the mechanical properties of REW joints were more stable than RSW joints. Optimized joints, i.e., REW joint under 7 kA welding current and RSW joint under 14 kA welding current, were used for microstructure, microhardness, and fatigue test, subsequently.

3.2 Microstructure

The microstructure of REW and RSW joints was investigated in detail (see Fig. 4). Fig. 4a, b show the macroscopic cross-section profiles of REW and RSW joints respectively. As in the case of the REW joints, the steel nuggets are formed at the rivet/steel sheet interface, and Al near the rivet body is melted owing to heat conduction [21]. The RSW joints consist of two separated nuggets, namely nuggets on the (i) steel side and (ii) Al side, which are inside the steel sheets and adjacent to the interface, respectively. Similar results have been reported for Al [11] or Mg [24] resistance spot welded to steel. In that case, the majority of Joule heat was generated in the steel, which has

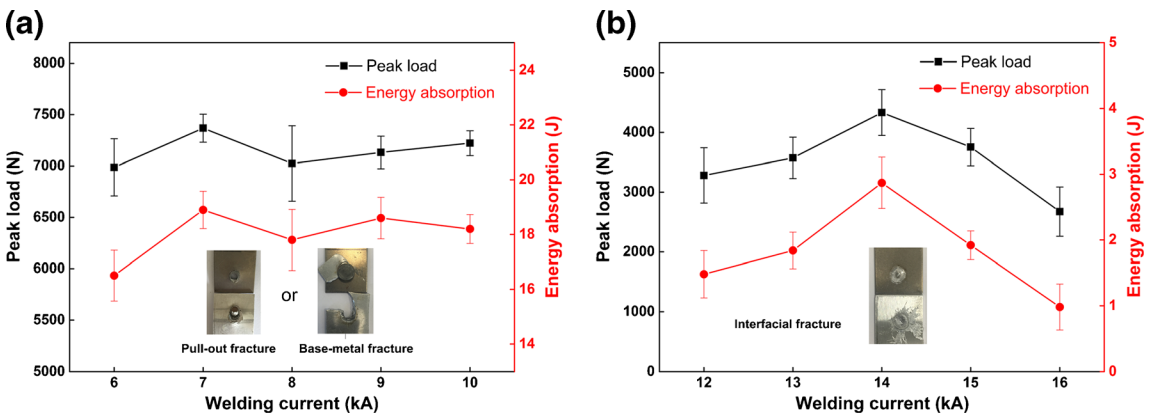

Fig. 3 Mechanical properties of **a** REW joints and **b** RSW joints under different welding currents

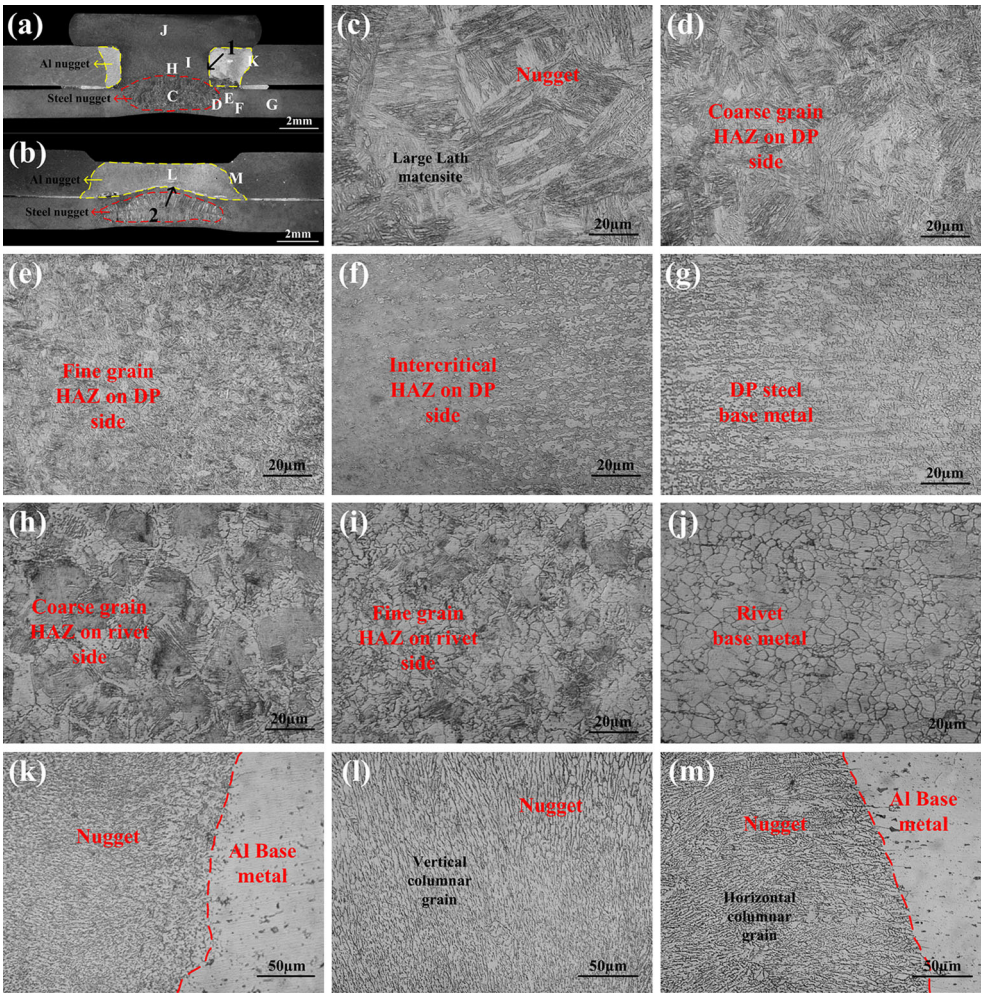

Fig. 4 Profiles of **a** REW joint and **b** RSW joint, and microstructure of **c**–**m** region C–region M

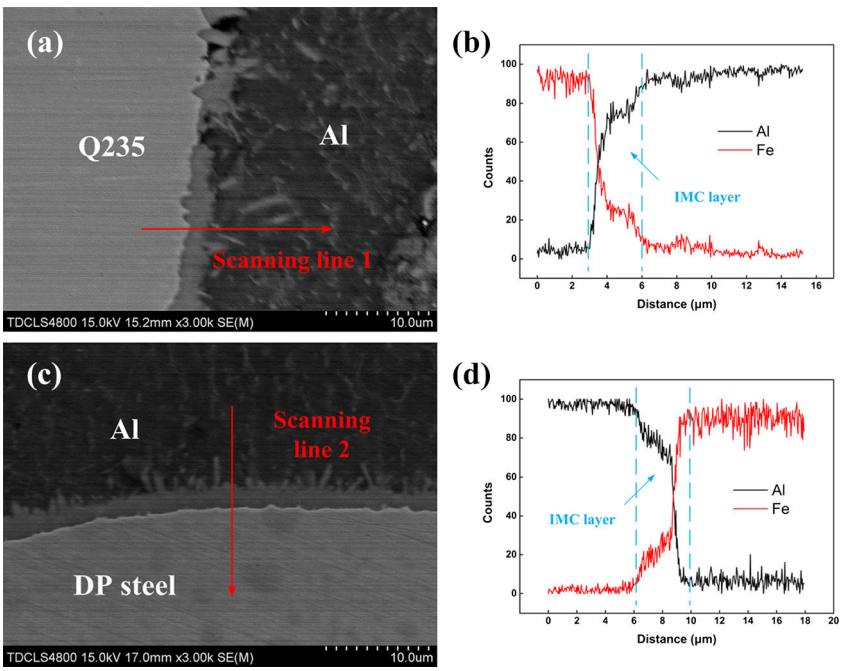

Fig. 5 IMC layers formed at the **a** rivet/Al interface and **c** Al/steel interface denoted by *black arrows* in Fig. 4, and the distribution of Fe and Al across the interface with scanning line **b** 1 and **d** 2

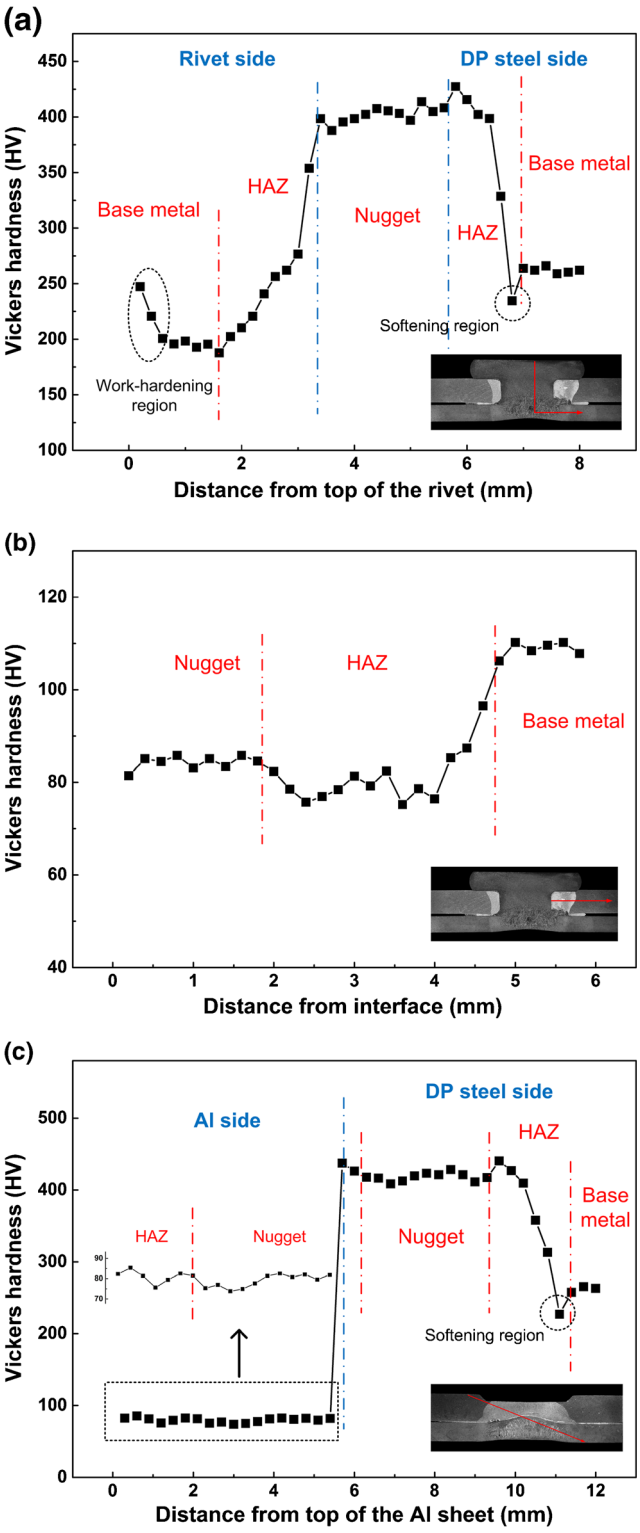

Fig. 6 Hardness distribution of the **a** steel in the REW joint, **b** Al in the REW joint, and **c** RSW joint

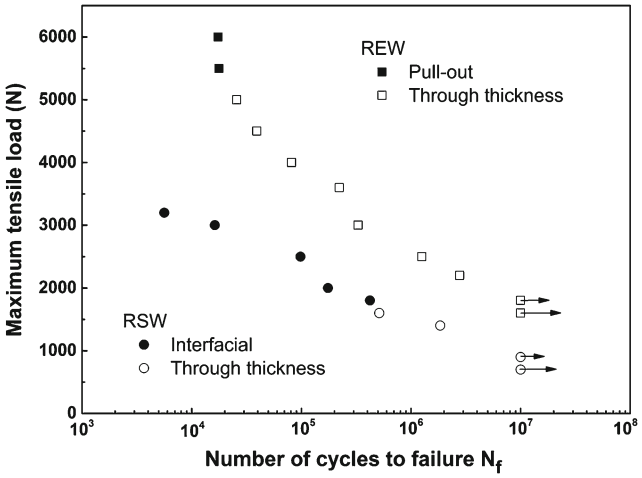

Fig. 7 Dependence of the maximum tensile load on the number of cycles to failure

a significantly higher resistivity than Al that acted as a cooling medium owing to its higher thermal conductivity. Therefore, the steel near the interface conducted a significant amount of heat to Al and the resulting relatively low temperature of this part prevented the melting point from being reached during welding [25]. Owing to remelting during welding, region C, which lies in the steel nugget, exhibits features consistent with an as-cast structure. The large lath martensite occurring in this region is attributed to the high cooling rate after welding [26]. Region D, which is the coarse-grained HAZ on the DP steel side, is also mainly composed of lath martensite, but the grain size is smaller than that of the nugget. The peak temperature in this region was significantly higher than the A_{C3} and, hence, the martensite was formed after rapid cooling, thereby leading to this smaller size. Martensite also occurs in region E, i.e., the fine-grained HAZ. However, the peak temperature in this region was only slightly higher than A_{C3}, resulting in less time (than that associated with region D) for grain growth, thereby leading to a fine-grained structure. The peak temperature of the intercritical HAZ (i.e., region D) lies between A_{C1} and A_{C3} and, hence, leads to incomplete austenization. Furthermore, the austenized part of the base metal was transformed into martensite after cooling, leading to a higher martensite content than that of the base metal. The base metal of the DP steel, denoted as region G, consists of two different phases namely, the black martensite phase and the white ferrite phase. Region G and region I are the coarse-grained HAZ and fine-grained HAZ, respectively, on the rivet side. The HAZ was overheated during welding, resulting in the formation of a Widmannstatten structure, where the grain size increases with decreasing distance from the nugget. Region G, i.e., the base metal of the rivet, is composed of pearlite and ferrite. Sharp boundaries occur in region K and region L, where the Al nugget on the left side is composed of columnar grains, and the right side is the Al base metal. Owing to the effect of the electrode pressure, the orientation of the columnar grains in the center of the nugget differs from that of the grains at the edge of the nugget (see Fig. 4m). The microstructure distribution in the steel side of the RSW joint is extremely similar to

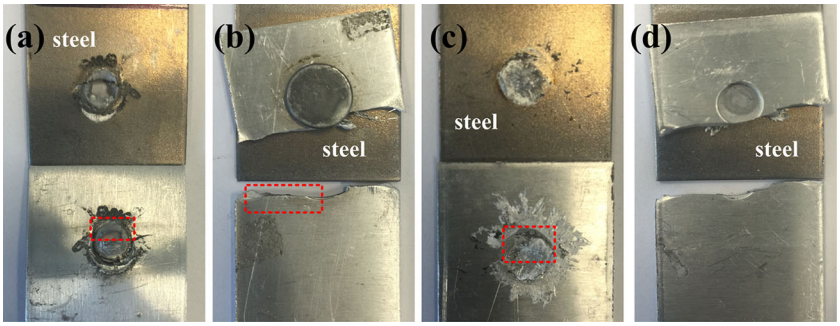

Fig. 8 Fatigue fracture appearances of the REW joints fracture at **a** 5500 N and 1.8×10^4 cycles and **b** 3000 N and 3.3×10^5 cycles and the RSW joints fracture at **c** 2500 N and 9.8×10^4 cycles and **d** 1400 N and 1.8×10^6 cycles

that of the REW joint, so the corresponding micrographs were not included in the paper.

The IMC layers in both joints (denoted by black arrows in Fig. 4) were analyzed via SEM. As the results in Fig. 5 show, an inconsistent 3-mm-thick IMC layer and a continuous 4-mm-thick IMC layer were formed at the rivet/Al and steel/Al interface, respectively.

3.3 Microhardness

The hardness distributions of REW and RSW joints are shown in Fig. 6. As Fig. 6a shows, the hardness of the rivet base metal is ~185 HV. The hardness at the top of the rivet is significantly higher than this value, because the rivet was punched by the electrode during welding and underwent work-hardening. The hardness of the HAZ on the rivet side is higher than that of the base metal and increases with decreasing distance from the nugget, owing to the overheated Widmannstatten structure formed in the region. The high hardness (average value: ~402 HV) of the nugget is attributed to the formation of large lath martensite. Furthermore, the hardness near the DP steel side is slightly higher than the hardness near the rivet side, because the carbon equivalent (CE) of the DP steel is higher than that of the rivet [27]. In addition, the coarse-grained HAZ at the DP steel side has smaller martensite grains and, therefore a slightly higher hardness than the nugget. The HAZ near the base metal consists of a softening region [26, 27], although there was no phase transition (the peak temperature was below A_{C1}) during welding. The microstructure in this region is quite similar to that of the base metal. However, the martensite in the base metal underwent a tempering process, leading to a decrease in hardness and, hence, this region may be described as a subcritical HAZ. The DP steel base metal has a hardness of ~262 HV. Moreover, the average hardness values of the Al nugget and base metal are 83 and 109 HV, respectively; the nugget underwent remelting and recrystallization, thereby resulting in a lower hardness than that of the base metal. The metal in the HAZ was not melted, but the temperature near the nugget was very high during welding, thereby reducing the positive effect of solution strengthening in the base metal. This occurrence, i.e., overaging, leads to a significant decrease in the hardness near the nugget. The hardness distribution of different regions in the RSW joint is quite similar to that of the REW joint (see Fig. 6c). However, owing to the finer grain size in this region (see in Fig. 4m), the hardness of the Al

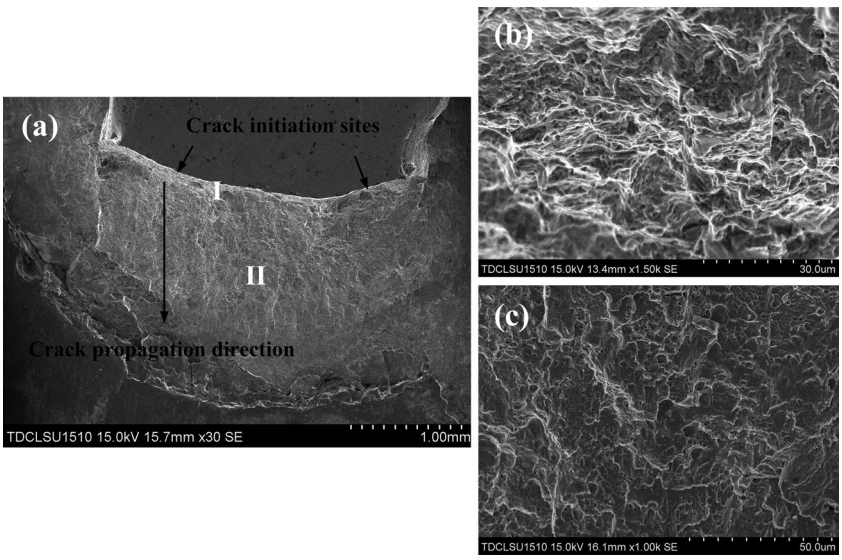

Fig. 9 Fracture surface morphology of the pull-out fracture mode **a** overall view and magnified view of **b** region I and **c** region II

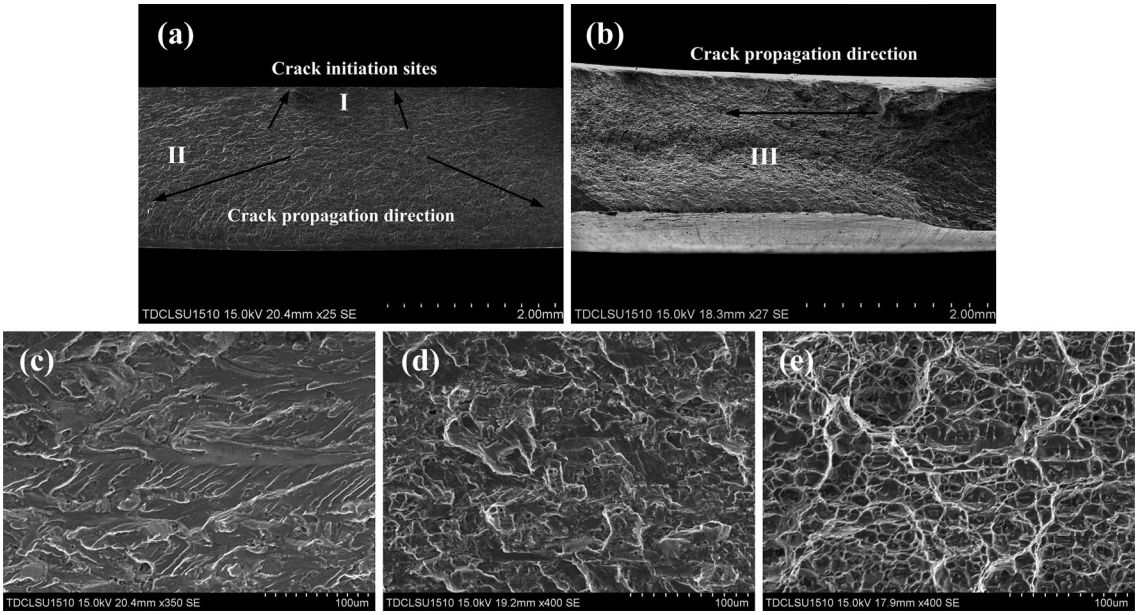

Fig. 10 Fracture surface morphology of the though-thickness fracture mode showing the overall view at the **a** center and **b** side; magnified view of **c** region I **d** region II, and **e** region III

nugget is slightly higher near the interface than in other regions. The average hardness of the steel nugget (418 HV) is higher than that of the steel nugget of the REW joint. This results from the higher CE of the DP steel and the overall higher nugget CE of the RSW joint compared to that of the REW joint.

3.4 Fatigue strength

The dependence of the maximum tensile load on the number of cycles to failure is shown in Fig. 7. Overall, the fatigue strength of the REW joint is significantly higher than that of the RSW joint. Defined as the runout load at 10^7 cycles, fatigue limits of 1800 and 900 N were obtained for the REW and RSW joints, respectively. Therefore, as in the case of previous studies, the Al/Fe dissimilar REW joint has a higher fatigue strength than the Al/Al similar RSW joint [28] and most Al/Fe dissimilar joints fabricated via various spot joining techniques (including RSW using an Al-Mg interlayer [11], friction stir spot welding [29], self-piercing riveting [30], and ultrasonic spot welding [31]).

3.5 Fatigue fracture morphology

In this study, a transition of fatigue fracture mode occurred in both the REW and RSW dissimilar joints. In the case of the REW joints, pull-out fracture (see Fig. 8a) occurred at high load levels ($P_{max} \geqq 5000$ N), while through-thickness fracture (see Fig. 8b) occurred at low load levels ($P_{max} \leq 5000$ N). In the case of the RSW joints, interfacial fracture (see Fig. 8c)

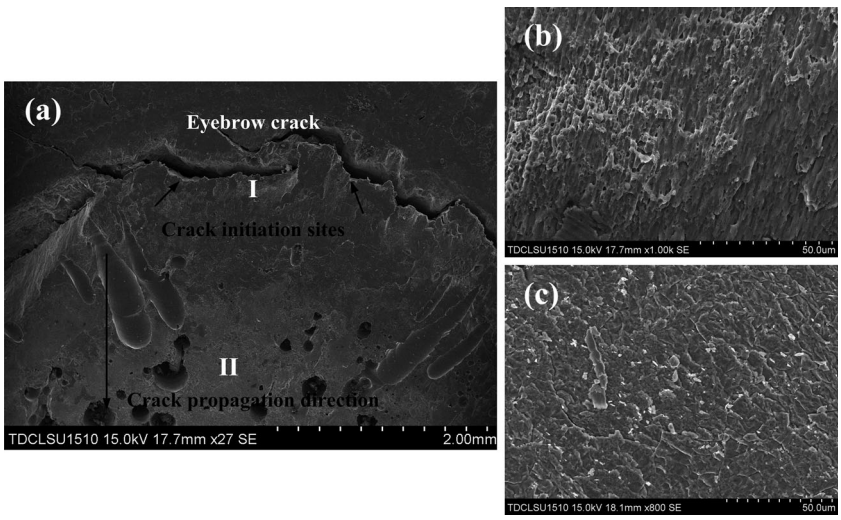

Fig. 11 Fracture surface morphology of the interfacial fracture mode **a** overall view and magnified view of **b** region I and **c** region II

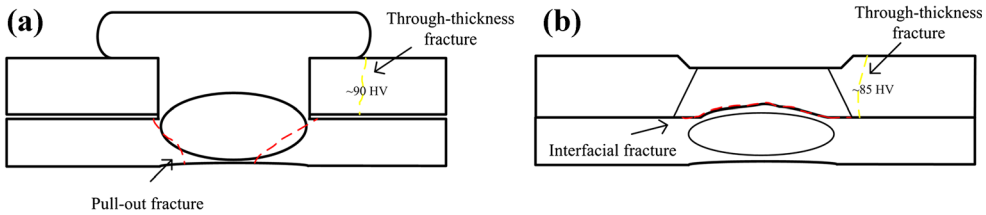

Fig. 12 Schematic illustration of fatigue fracture paths of **a** REW joint and **b** RSW joint

occurred at high load levels (P_{max}≧1600 N), whereas through-thickness fracture (see Fig. 8d) occurred at low load levels ($P_{max} \leq 1600$ N).

Figure 9a shows an overall view of the pull-out fracture mode. The crack was initiated at the surface of the steel sheet. A magnified view of the crack initiation site (see Fig. 9b) reveals a rough slightly striated surface. The crack propagated along the thickness direction, and the corresponding magnified view (see Fig. 9c) revealed a complex fracture surface, which consists of both dimples and planes.

Figure 10a, b show the overall view of the through-thickness fracture mode. The crack was initiated at the center and edge of the Al sheet, and was accompanied by significant fatigue striations, as shown in Fig. 10c. The crack then propagated stably through the thickness and along the width of the sheet, thereby resulting in a brittle surface (see Fig. 10d). In the final stage, crack propagation was unstable and rapid, as evidenced by the occurrence of dimples on the surface (see Fig. 10e). All of the through-thickness fracture modes yielded similar surface morphology.

Figure 11a shows the overall view of the interfacial fracture mode. An eyebrow crack formed at the crack initiation site. In addition, as shown in Fig. 11b, elongated dimples occurred at the crack initiation site. The crack propagated along the interface, where the fracture surface is composed of cleavage planes. This indicates that the crack propagated rapidly during the final stage.

3.6 Fatigue fracture mechanisms

Figure 12 summarizes the fatigue fracture paths of dissimilar joints. For the REW joint, nugget rotation occurred at high load levels (P_{max}≧5000 N), thus, the tensile shear load partly transformed to the component load which is perpendicular to the nugget [32]. Meantime, severe microstructure change led to the stress concentration at the edge of the nugget. These two factors allowed the crack initiating at the edge of the nugget and finally resulted in the pull-out fracture. While at low load levels ($P_{max} \leq 5000$ N), the nugget rotation was small, so the component load perpendicular to the nugget was not higher enough to initiate cracks. With the action of cyclic tensile load, the cracks initiated at the hardness mutation area of Al, where the stress concentration was most serious in the Al sheet, and through-thickness fracture occurred. For the RSW joint, at high load levels (P_{max}≧1600 N), an eyebrow crack formed at the crack initiation site owing to the component load perpendicular to the nugget [33]; because of the insufficient load-bearing capacity of the IMC layer, the crack would quickly propagate through the interface, leading to interfacial fracture. While at low load levels ($P_{max} \leq 1600$ N), the IMC layer was able to endure the shear load, so through-thickness fracture occurred at very high load cycles.

4 Conclusions

A 6061-T6 aluminum alloy and electro-galvanized DP780 steel were dissimilar welded via novel resistance element welding. The microstructure, microhardness, fatigue strength, and fatigue fractographs of REW joints were obtained and compared with RSW joints. The main findings of this work can be summarized as follows:

1. REW exhibited outstanding properties during dissimilar Al/steel joining. Under optimal conditions, the tensile shear strength (7368 N) and energy absorption (18.9 J) of the REW dissimilar joints were 70% and over six times higher, respectively, than those of the RSW joints. This is indicative of the excellent integrated mechanical properties of the REW joints.
2. Nuggets formed at the interface of the rivet and steel in the REW joints. Two separate nuggets formed in the RSW joints. The microstructure of the joints varied with the distance from the center of the nugget, and different microhardnesses were obtained for different microstructures. IMC layers formed at the interface of the Al/rivet interface and Al/steel interface in the REW joints and RSW joints, respectively.
3. The fatigue limit of the REW joints (1800 N) was significantly higher than that of the RSW joints (900 N). Overall, the fatigue strength of the REW joints was superior to that of the Al/Al RSW joints and most of the Al/steel dissimilar spot joints. The fatigue fracture modes of the REW and RSW joints were dependent on the load levels and, at high load levels, these joints underwent pull-out and interfacial fracture, respectively. However, at low load levels, both joints underwent through-thickness fracture.

Acknowledgements The authors gratefully acknowledge the support of the National Natural Science Foundation of China under Grant No.

51405334 and Grant No. 51405335, and the Provincial Science and Technology Program of Guangdong Province under Grant No.2013B090600149.

References

1. Frondel M, Schmidtand CM, Vance C (2011) A regression on climate policy: the European Commission's legislation to reduce CO_2 emissions from automobiles. Transpor Res Part A 45(10):1043–1051
2. Manladan SM, Yusof F, Ramesh S, Fadzil M, Luo Z, Ao S (2016) A review on resistance spot welding of aluminum alloys. Int J Adv Manuf Technol. doi:10.1007/s00170-016-9225-9
3. Hayat F, Sevim I (2012) The effect of welding parameters on fracture toughness of resistance spot-welded galvanized DP600 automotive steel sheets. Int J Adv Manuf Technol 58:1043–1050
4. Hayat F (2011) Resistance spot weldability of dissimilar materials: BH180-AISI304L steels and BH180-IF7123 steels. J Mater Sci Technol 27(3):1047–1058
5. Shah LH, Ishak M (2014) Review of research progress on aluminum–steel dissimilar welding. Mater Manuf Process 29(8):928–933
6. Ozaki H, Kutsuna M (2009) Laser roll welding of dissimilar metal joint of low carbon steel to aluminium alloy using 2KW fiber laser. Weld Int 23(5):345–352
7. Qiu R, Iwamoto C, Satonaka S (2009) Interfacial microstructure and strength of steel/aluminium alloy joints welded by resistance spot welding with cover plate. J Mater Process Technol 209:4186–4193
8. Sun D, Zhang Y, Liu Y, Gu X, Li H (2016) Microstructures and mechanical properties of resistance spot welded joints of 16Mn steel and 6063-T6 aluminum alloy with different electrodes. Mater Des 109:596–608
9. Zhang W, Sun D, Han L, Liu D (2014a) Interfacial microstructure and mechanical property of resistance spot welded joint of high strength steel and aluminium alloy with 4047 AlSi12 interlayer. Mater Des 57:186–194
10. Zhang W, Sun D, Han L, Li Y (2015) Optimised design of electrode morphology for novel dissimilar resistance spot welding of aluminium alloy and galvanised high strength steel. Mater Des 85:461–470
11. Ibrahim I, Ito R, Kakiuchi T, Uematsu Y, Yun K, Matsuda C (2016) Fatigue behaviour of al/steel dissimilar resistance spot welds fabricated using Al–Mg interlayer. Sci Technol Weld Join 21(3):223–233
12. Arghavani MR, Movahedi M, Kokabi AH (2016) Role of zinc layer in resistance spot welding of aluminium to steel. Mater Des 102:106–114
13. Dong H, Hu W, Duan Y, Wang X, Dong C (2012) Dissimilar metal joining of aluminium alloy to galvanized steel with Al-Si, Al-Cu, Al-Si-Cu and Zn-Al filler wires. J Mater Process Technol 212:458–464
14. Cao R, Huang Q, Chen JH, Wang PC (2014) Cold metal transfer spot plug welding of AA6061-T6-to-galvanized steel for automotive applications. J Alloys Compd 585:622–632
15. Lan S, Liu X, Ni J (2016) Microstructural evolution during friction stir welding of dissimilar aluminum alloy to advanced high-strength steel. Int J Adv Manuf Technol 82:2183–2193
16. Mirza FA, Macwan A, Bhole SD, Chen DL, Chen XG (2016) Effect of welding energy on microstructure and strength of ultrasonic spot welded dissimilar joints of aluminum to steel sheets. Mater Sci Eng A 668:73–85
17. Lou M, Li YB, Wang Y, Wang B, Lai X (2009) Self-piercing riveting of high tensile strength steel and aluminium alloy sheets using conventional rivet and die. J Mater Process Technol 209:3914–3922
18. Jiang T, Liu ZX, Wang PC (2015) Quality inspection of clinched joints of steel and aluminum. Int J Adv Manuf Technol 76:1393–1402
19. Miles M, Hong ST, Woodward C, Jeong YH (2013) Spot welding of aluminium and cast iron by friction bit joining. Int J Prec Eng Manuf 14(6):1003–1006
20. Meschut G, Janzen V, Olfermann T (2014) Innovative and highly productive joining technologies for multi-material lightweight car body structures. J Mater Eng Perform 23(5):1515–1523
21. Ling Z, Li Y, Luo Z, Feng Y, Wang Z (2016) Resistance element welding of 6061 aluminum alloy to uncoated 22MnMoB boron steel. Mater Manuf Process 31(16):2174–2180
22. AWS D17.2 (2007) Specification for resistance welding for aerospace applications
23. Pouranvari M, Marashi SPH (2013) Critical review of automotive steels spot welding: process, structure and properties. Sci Technol Weld Join 18(5):361–403
24. Feng Y, Li Y, Luo Z, Ling Z, Wang Z (2016) Resistance spot welding of Mg to electro-galvanized steel with hot-dip galvanized steel interlayer. J Mater Process Technol 236:114–122
25. Wan Z, Wang HP, Wang M, Carlson BE, Sigler DR (2016) Numerical simulation of resistance spot welding of Al to zinc-coated steel with improved representation of contact interactions. Inter J Heat Mass Transfer 101:746–763
26. Liu Y, Dong D, Wang L, Chu X, Wang P, Jin M (2015) Strain rate dependent deformation and failure behavior of laser welded DP780 steel joint under dynamic tensile loading. Mater Sci Eng A 627:296–305
27. Zhang H, Wei A, Qiu X, Chen J (2014b) Microstructure and mechanical properties of resistance spot welded dissimilar thickness DP780/DP600 dual-phase steel joints. Mater Des 54:443–449
28. Florea RS, Bammann DJ, Yeldell A, Solanki KN, Hammi Y (2013) Welding parameters influence on fatigue life and microstructure in resistance spot welding of 6061-T6 aluminum alloy. Mater Des 45:456–465
29. Uematsu Y, Tokaji K, Tozaki Y, Nakashima Y, Shimizu T (2011) Fatigue behaviour of dissimilar friction stir spot welds between A6061-T6 and low carbon steel sheets welded by a scroll grooved tool without probe. Fatigue Fract Eng Mater Struct 34(8):581–591
30. Huang L, Shi Y, Guo H, Su X (2016) Fatigue behavior and life prediction of self-piercing riveted joint. Int J Fatigue 88:96–110
31. Pater VK, Bhole SD, Chen DL (2014) Ultrasonic spot welding of aluminum to high-strength low-alloy steel: microstructure, tensile and fatigue properties. Metall Mater Trans A 45A(4):2055–2066
32. Uematsu Y, Tokaji K (2009) Comparison of fatigue behavior between resistance spot and friction stir spot welded aluminium alloy sheets. Sci Technol Weld Join 14(1):32–71
33. Shen Z, Ding Y, Chen J, Gerlich AP (2016) Comparison of fatigue behavior in Mg/Mg similar and Mg/steel dissimilar refill friction stir spot welds. Int J Fatigue 92:78–86